Electronic Supplementary Material (ESI) for Journal of Materials Chemistry A.

Electronic Supplementary Information (ESI):

Surfactant exfoliated 2D hexagonal boron nitride (2D-hBN): role of surfactant upon the electrochemical reduction of oxygen and capacitance applications

Aamar F. Khan[1], Michael P. Down[1], Graham C. Smith[2], Christopher W. Foster[1],

and Craig E. Banks[1]*

[1]: *Faculty of Science and Engineering, Manchester Metropolitan University, Chester Street,*
Manchester M1 5GD, UK.

[2]: *Faculty of Science and Engineering, Department of Natural Sciences, University of Chester,*
Thornton Science Park, Pool Lane, Ince, Chester CH2 4NU, UK.

*To whom correspondence should be addressed.

Email: c.banks@mmu.ac.uk; Tel: ++(0)1612471196; Fax: ++(0)1612476831

Website: www.craigbanksresearch.com

A systematic approach to characterising the capacitance of an electrode pair in a parallel circuit with a capacitor is presented here. In order to best describe the benefit of this approach, the principles of capacitor theory should be first understood. A specific example can be used, with three capacitors, which illustrates how utilising a parallel circuit can improve the interpretation of the experimental results. In this example, we consider three capacitors of capacitance C_1, C_2 and C_3. We will assume that the capacitor C_1 is the supercapacitor such that $C_1 = C_{supercapacitor}$. The first case, where the capacitors are connected in parallel, as shown in ESI Figure 1. In this case the potential across the capacitors is the same:

$$V = V_2 = V_3 = V_{Supercapacitor} \tag{1}$$

and as such the total charge is distributed equally across the capacitors:

$$Q = Q_2 = Q_3 = Q_{Supercapacitor} \tag{2}$$

and consequently:

$$C_{total}V = C_2V_2 + C_3V_3 + C_{Supercapacitor}V_{Supercapacitor} \tag{3}$$

but from ESI equation 1 we have:

$$C_{total}V = C_2V + C_3V + C_{Supercapacitor}V \tag{4}$$

and finally

$$C_{total} = C_2 + C_3 + C_{Supercapacitor} \tag{5}$$

In this example, the total capacitance of the parallel circuit is the sum of all the capacitances of each of the parallel branches.

The second case is where there are three capacitors in series as shown in ESI Figure 1B. In this case the potential is split between each of the components in series:

$$V = V_2 + V_3 + V_{Supercapacitor} \tag{6}$$

and

$$V = V_2 + V_3 + V_{Supercapacitor} \tag{7}$$

therefore

$$\frac{Q}{C_{total}} = \frac{Q}{C_2} + \frac{Q}{C_3} + \frac{Q}{C_{supercapacitor}} \tag{8}$$

and finally

$$\frac{1}{C_{total}} = \frac{1}{C_2} + \frac{1}{C_3} + \frac{1}{C_{supercapacitor}} \tag{8}$$

In this case the total capacitance of the series circuit is the sum of the inverse capacitances of the components.

If we consider the effect of this comparison on the analysis of the capacitive properties of the supercapacitor, we can see the benefit of analysing the properties in a circuit of know capacitance. ESI Figure 2 shows the various arrangements for analysis of the supercapacitor in parallel with a 100 µF capacitor. Either a single 100 µF capacitor is utilised in parallel shown in ESI Figure 2B or a variable capacitor system is set to 100 µF in parallel, shown in ESI Figure 2A. The effect this has on the observed charging cycle and the interpretation of the *dV/dt* are shown in ESI Figure 2C. As a commercial grade capacitor has a nominally linear response, the resulting curve is a combination of a linear curve and the plateauing 'shark-fin' shaped curve that is often seen in experimental supercapacitor characterisation. The resulting curve still presents a relatively curved shape and as such poses the same problem as before, in that the determination of where to take the gradient for the characteristic capacitance is undefined. In order to address this, further evaluations of varying parallel capacitances are investigated.

Through increasing the parallel capacitance, the effect on the nominal gradient of the charging cycles can be seen. ESI Figure 3 shows the arrangements for measuring in parallel with a 200 µF capacitor, or two 100 µF capacitors, which as shown previously are the same. In this case, the line is significantly smoother still and straighter. Increasing the parallel capacitance further still, to 620 µF, shown in ESI Figure 4, the charge cycles are near linear in behaviour. As a result, the gradient of the whole line can be utilised to determine the capacitive properties of the system, and equation 5 from the main body of text can be used to interpret the capacitance for the working electrode.

The result of this analysis is a systematic approach for providing a true value of the capacitance of an electrode without the risk of misinterpretation of the data. Also by utilising the component in a system the approach to the analysis of electrode properties, the set-up is limited to a 2-wire/electrode analysis, which is commercially more useful in terms of supercapacitors. This is a benefit, also, as there is yet to be a standardized approach to such analysis. This develops a uniform approach for all researchers, providing a system that improves repeatability and cohesion amongst the field. The approach consists of the following steps;

1) Perform charge/discharge cycles with the system alone, without any parallel capacitance;
2) Interpret the capacitance without the circuit;
3) Insert the variable capacitor/capacitor circuit in parallel with a low capacitance, of the order of the value extracted from the interpretation without the circuit in steps 1) and 2);
4) Re-interpret the capacitance from the resulting charge cycle, with the parallel circuit in place.
5) If the charge properties are still not linear increase the capacitance until a linear signal is achieved;
6) Interpret the *true capacitance* from the resulting linear charge response.

ESI Figure 1

Capacitance circuits for the three-capacitor system, A) in parallel and B) in series.

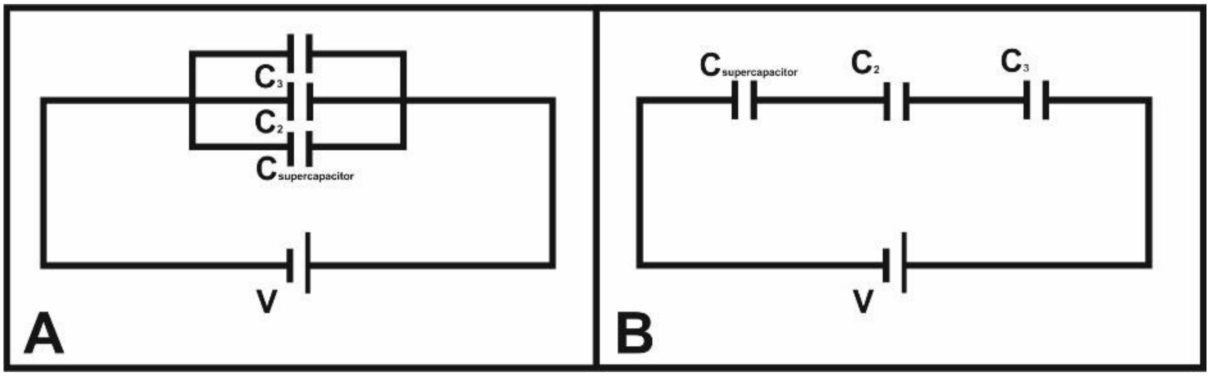

ESI Figure 2

Evaluation of the capacitance of the supercapacitor integrated into a parallel circuit for 100 μF.

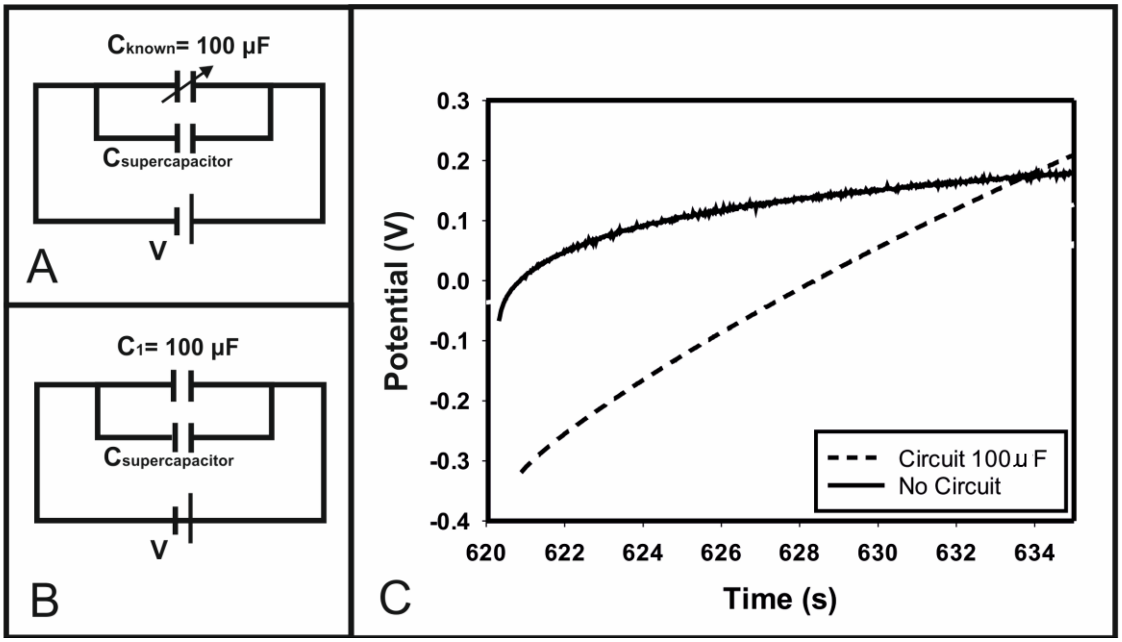

ESI Figure 3

Evaluation of the capacitance of the supercapacitor integrated into a parallel circuit for 200 μF.

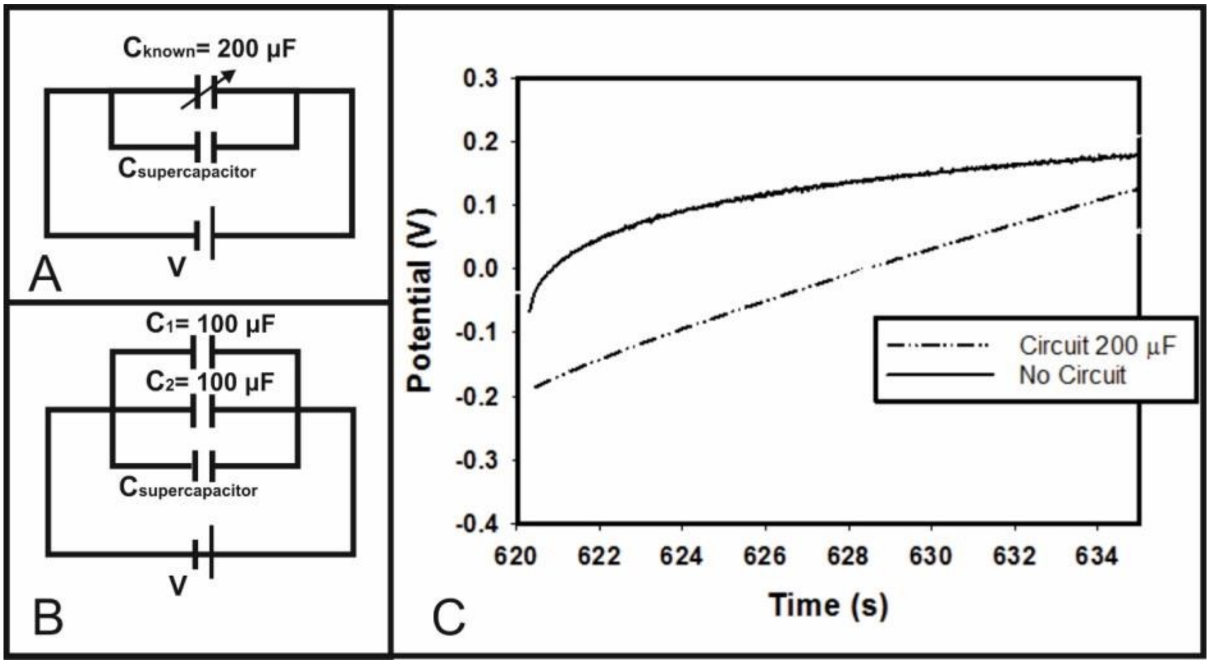

ESI Figure 4

Evaluation of the capacitance of the supercapacitor integrated into a parallel circuit for 620 μF.

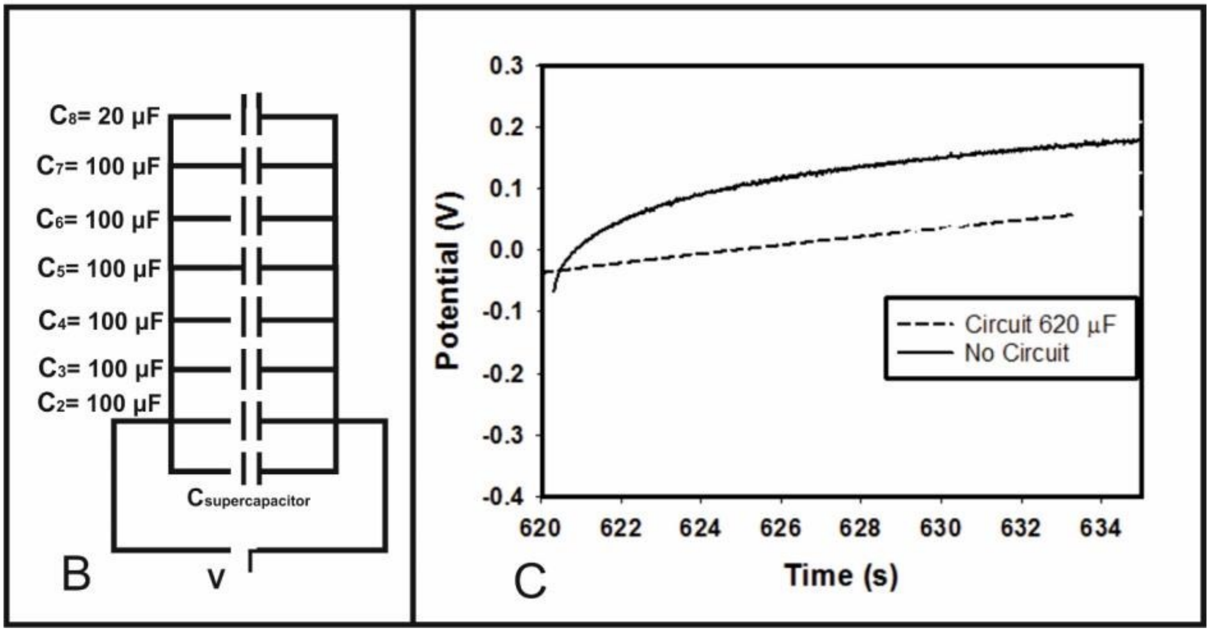

Exfoliation/synthesis of 2D-hBN

The 2D-hBN utilised throughout this work was synthesised *via* a surfactant based liquid exfoliation, sonication and centrifugation methodology. Liquid exfoliation was performed by adding bulk h-BN powder into an aqueous solution of sodium cholate hydrate (SC: concentration, 6 g/L) contained within a 100 mL beaker. The resulting dispersion of bulk h-BN comprised a concentration of 30 g L^{-1}. This dispersion was then sonicated in a sonication bath (Ultrawave, UK) (60 % Amplitude) for 1 hour, prior to a centrifugation step that was performed at 5000 rpm for 90 minutes. Following centrifugation, the corresponding supernatant was discarded and the resulting sediment was re-agitated/dispersed into aqueous SC (2 g/L, 100 mL). Next, the said re-agitated sediment underwent sonication in a sonication bath (Ultrawave, UK) (60 % Amplitude) for a further 5 hours. Upon completion of the sonication treatment, the solution was separated into 20 mL aliquots before each sample was centrifuged at 2000 rpm for 90 mins (separately). The sediment from this process contained un-exfoliated h-BN and was consequently discarded, with the remaining supernatant being subjected to a further centrifugation period at 5000 rpm for 90 minutes. Finally, the forthcoming supernatant was removed and found to contain the 2D-hBN nanosheets that are utilised herein.

Optical band gap calculation applied towards 2D-hBN

The Tauc equation: $\omega^2\varepsilon = (h\omega - E_g)^2$ was utilised to determine the optical band gap E_g for surfactant-exfoliated 2D-hBN.[1] Where ε is the optical absorbance, h is Planck's constant, and $\omega = 2\pi/\lambda$ is the angular frequency of the incident radiation (λ is the wavelength). Thus, a plot of $\varepsilon^{1/2}/\lambda$ versus $1/\lambda$ results in a straight line at the absorption range. Hence, the intersection point with the x axis is $1/\lambda_g$ (λ_g is defined as the gap wavelength). Finally, the optical band gap can be calculated utilising the equation $E_g = hc/\lambda_g$.[2] Consequently, ESI Figure 6 illustrates that the surfactant-exfoliated 2D-hBN exhibits an absorption peak at 203 nm and a plot of $\varepsilon^{1/2}/\lambda$ *vs*. $1/\lambda$ can be constructed (inset ESI Figure 6). Therefore, the calculated gap wavelength (λ_g) relates to 221.2 nm, with a corresponding optical band gap of 5.61 eV indicating that 2-4 layer 2D-hBN is present in solution.[2]

ESI Figure 5

Diagram showing how screen-printed electrodes (SPEs) are utilised to electrically wire the 2D-hBN materials. Typical SPEs consisting of a graphite working electrode, (WE, 3mm diameter), a graphite counter electrode, (CE) and an Ag/AgCl reference electrode (RE). Note, only the working electrode was utilised throughout the study with the others cut away with sharp scissors and external CE and REF utilised; this permits ease of surface modification and the external REF allows comparison to the literature.

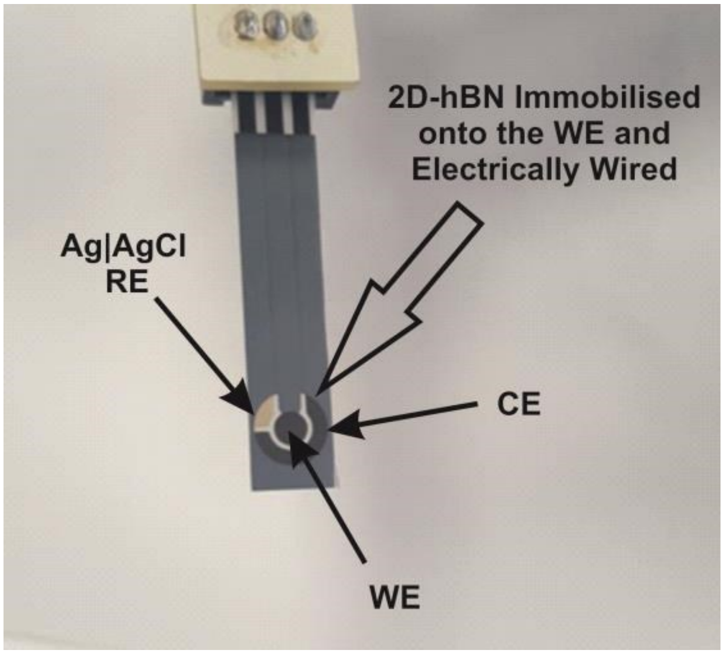

ESI Figure 6

A typical UV-visible absorption spectra of surfactant-exfoliated 2D-hBN nanosheets, where the inset shows the corresponding plot of $\varepsilon^{1/2}/\lambda$ *vs*. $1/\lambda$.

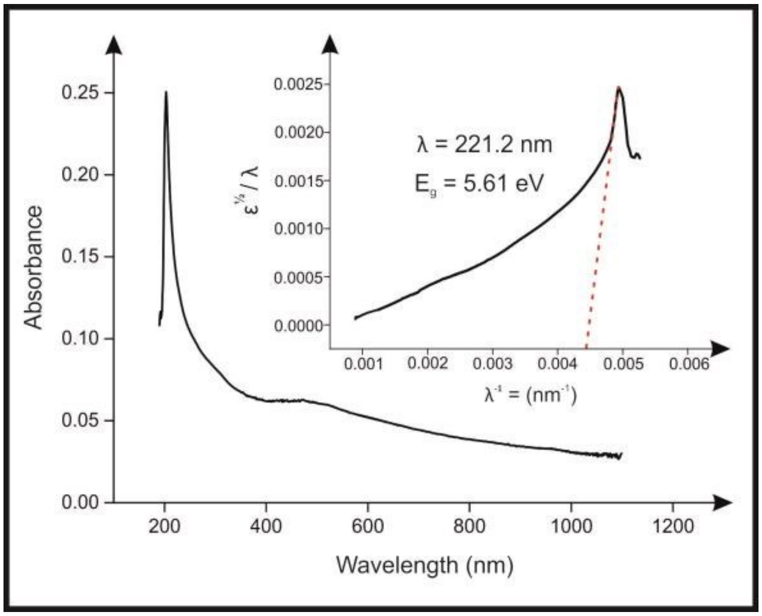

ESI Figure 7

XPS survey spectrum for a sample of the surfactant-exfoliated 2D-hBN following deposition onto a Si (111) wafer.

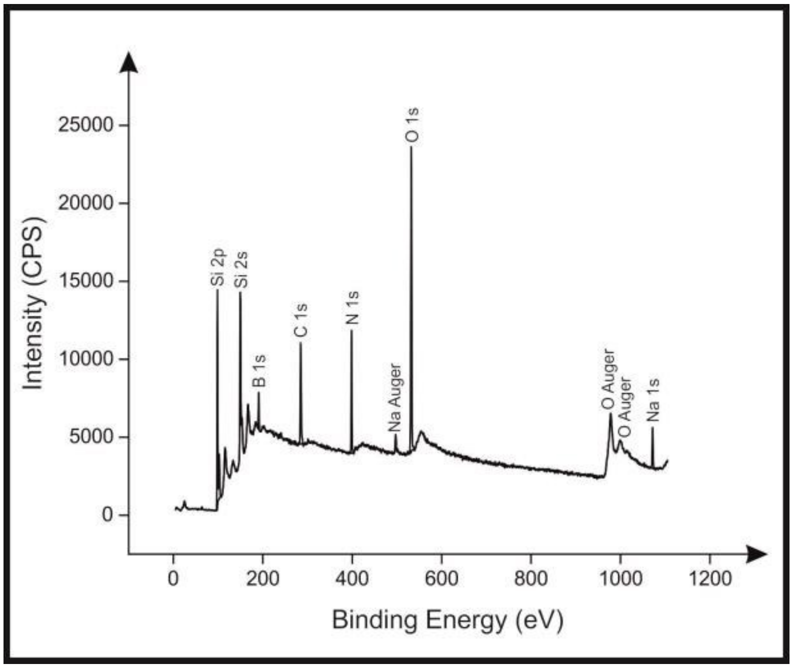

ESI Figure 8

Curve fitted XPS spectra of surfactant-exfoliated 2D-hBN deposited upon a Si (111) wafer. (A) illustrates XPS spectra of the B atom and spectra (B) is that of the N atom.

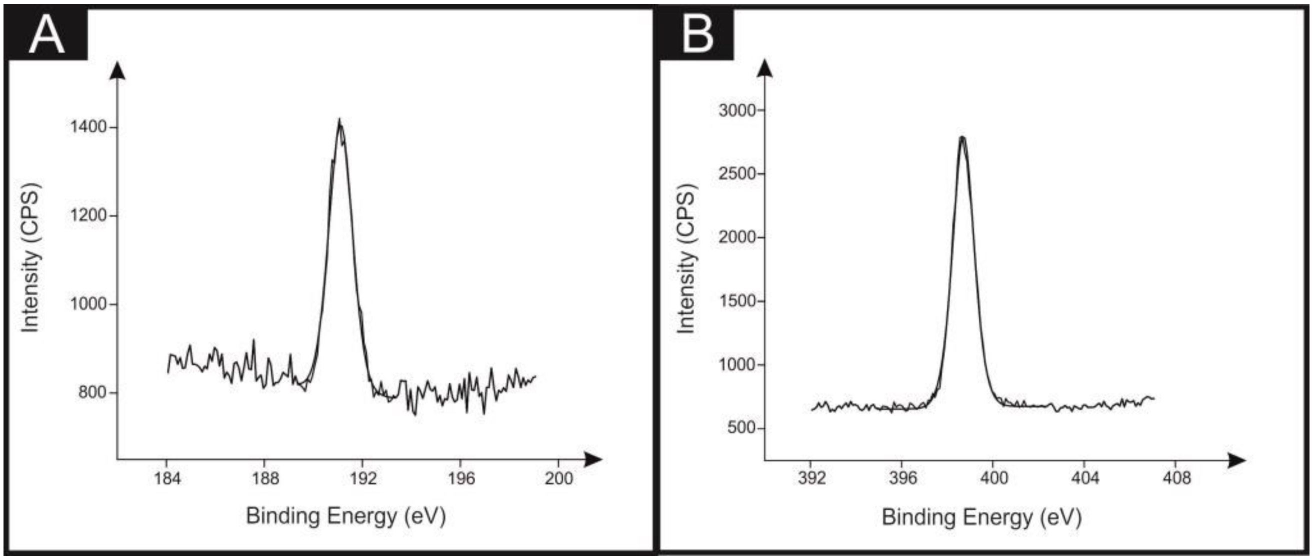

ESI Table 1

A summary depicting the composition of surfactant-exfoliated 2D-hBN layer dried from sodium cholate suspension onto Si(111), following analysis of XPS spectra. Note that the analysis includes data from the 2D-hBN and the sodium cholate residue.

Element	Atom % Layer composition
O 1s	26.4
C 1s	31.4
Na 1s	2.8
B 1s	19.8
N 1s	19.6

ESI Figure 9

XRD spectra of the surfactant-exfoliated 2D-hBN deposited onto a glass slide between 20 and 45 2θ, exhibiting a characteristic peak at 26.7°**.**

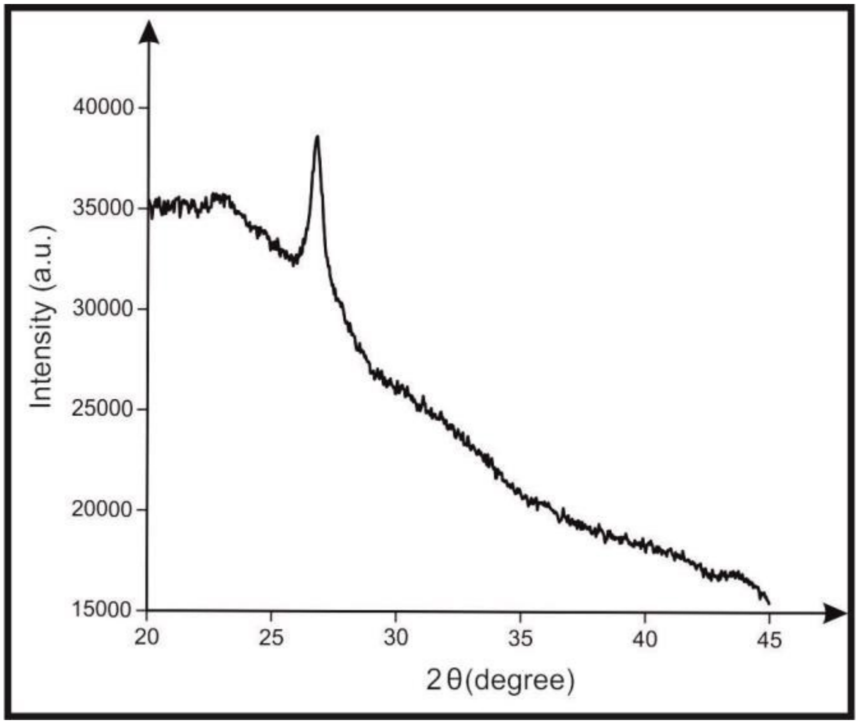

Material Characterisation of pristine 2D-hBN

The physicochemical characterisation of the pristine 2D-hBN utilised in this work is provided through TEM, SEM, XPS, EDX, XRD and Raman spectroscopy. Typical TEM images are depicted in ESI Figure 10 where it can be observed that pristine 2D-hBN platelets have an average (lateral) particle size of *ca*. 200 nm, which is in agreement with the commercial manufacturer.[3] Furthermore, SEM images were obtained to assess how the pristine 2D-hBN platelets prefer to reside upon SPE surfaces. ESI Figure 11 depicts an SEM image of pristine 2D-hBN (324 ng) residing upon an SPE, where pristine 2D-hBN platelets are visible as discs of particle size *ca*. 200 nm, that collect preferentially around contours and ridges upon the SPE surface, similar to that of surfactant-exfoliated 2D-hBN (Figure 1D).

XPS analysis was next performed on the pristine 2D-hBN and is depicted in ESI Figure 12. Note that the analysis was conducted on a thin layer of pristine 2D-hBN, dried from an ethanol suspension on a Si (111) substrate and therefore the results include contributions from the underlying Si wafer, its surface oxide and any adventitious contaminants as well as from the pristine 2D-hBN and the ethanol residue. The XPS spectra showed the presence of a single component at 190.8 eV in the B 1s spectrum and the N 1s spectrum exhibited a main peak at 398.4 eV, with both in good agreement to previous literature.[4] A weak (minor) component in the N 1s spectrum at *ca*. 400.2 eV was evident and most likely originated from atmospheric contamination on the underlying silicon, Si (111) substrate. Thus, the results are fully consistent with pristine 2D-hBN immobilised upon a Si (111) substrate. The stoichiometry of 1:1 for B:N is noted and the binding energies for the B 1s and N 1s photoelectron peaks agree well with the expected values for pristine 2D-hBN. ESI Table 2 exhibits the full surface composition of the dried ethanol suspension of pristine 2D-hBN on Si (111) from the XPS analysis. The C and O present are likely a result of residuals from the ethanol used to disperse the 2D-hBN. The presence of a C-O component in the C 1s spectrum (not shown) confirmed this. The Na and Ca were attributed to the concentration of organic Na- and Ca-containing contaminants in the ethanol. The Si and a proportion of the O originated form the Si (111) wafer substrate, which typically has thin surface oxide of approximately 1.5 nm thickness. The XPS analysis confirmed the presence of stoichiometric pristine 2D-hBN in the commercially obtained material.

It has previously been shown that metallic impurities in carbon nanotubes can contribute to the electrocatalysis seen at some nanotube-modified electrodes.[5] Thus, it is important to consider the possible presence of metallic impurities for the case of pristine 2D-hBN, which if present, may contribute to the response observed towards the ORR. EDX analysis was performed on a single platelet of pristine 2D-hBN (see ESI Figure 13) to further establish its elemental composition, where it was indicated to be comprised of 11.40% atomic boron and 9.93% atomic nitrogen. This is in agreement with the XPS obtained that shows the stoichiometry between B:N is *ca.* 1:1. Further scrutiny of the EDX data reveals a 78.67% contribution/component of atomic Silicon (Si), which as discussed above originates from the substrate upon which pristine 2D-hBN is immobilised. This confirms that there are no impurities within our commercially obtained samples, therefore the response is not dominated by such metallic constituents, but rather is due solely to that of the pristine 2D-hBN present.

XRD was performed on the pristine 2D-hBN with corresponding spectra depicted in ESI Figure 14, indicating that pristine 2D-hBN crystals are oriented in the (002) direction with a characteristic peak observed at 26.7°, in agreement with an independent literature report.[6]

Finally, the commercially procured pristine 2D-hBN was characterised using Raman spectroscopy. ESI Figure 15A shows Raman spectra of immobilised pristine 2D-hBN upon a silicon wafer, which gives rise to a characteristic Raman peak at 1365 cm^{-1}, which is due to the E_{2g} phonon mode.[7] This is in good agreement to an independent literature report,[7] indicating that the immobilised sample upon the silicon wafer consists of *ca.* 2 – 4 layers of pristine 2D-hBN. Note however, it is not possible to observe the Raman peak of pristine 2D-hBN upon graphitic electrodes due to overlapping signals occurring between pristine 2D-hBN and graphite. Hence, we cannot refer to the pristine 2D-hBN modified electrode in terms of the number layers immobilised upon it, but rather the mass of pristine 2D-hBN that has been immobilised each time. Next, several masses of pristine 2D-hBN were immobilised upon SPEs. These modified SPEs were characterised using Raman spectroscopy (mapping) to ensure full electrode coverage of pristine 2D-hBN. ESI Figures 15B and 15C show Raman map comparisons of an unmodified and a 324 ng pristine 2D-hBN modified SPE. ESI Figure 15B shows a smooth / uniform surface, yet ESI Figure 15C shows several areas, appearing as black dots (and generally has a darker grey background intensity), that are indicative of 2D-hBN immobilisation given that the Raman intensities were recorded at the wavenumber corresponding to the peak observed in ESI Figure 15A. The Raman maps indicate a significant coverage of *ca*. 2 layer (thin layer) pristine 2D-hBN on the electrode surface (with some areas that are darker in colour (higher Raman intensity) indicating occasional thicker regions (≥ 2

– 4 layers).[27] It is clear that following pristine 2D-hBN modification *via* drop casting, a complete coverage is achieved and thus the electrochemical profiles associated with pristine 2D-hBN modified electrodes are due to the pristine 2D-hBN and not the underlying electrode surface.

ESI Figure 10

Typical TEM images of commercially procured pristine 2D-hBN deposited onto a holey carbon film supported upon a Cu TEM grid (A), and at a higher magnification (B). Scale bars are 200 nm (A) and 100 nm (B). Images obtained using a 200 kV primary beam under bright-field conditions.

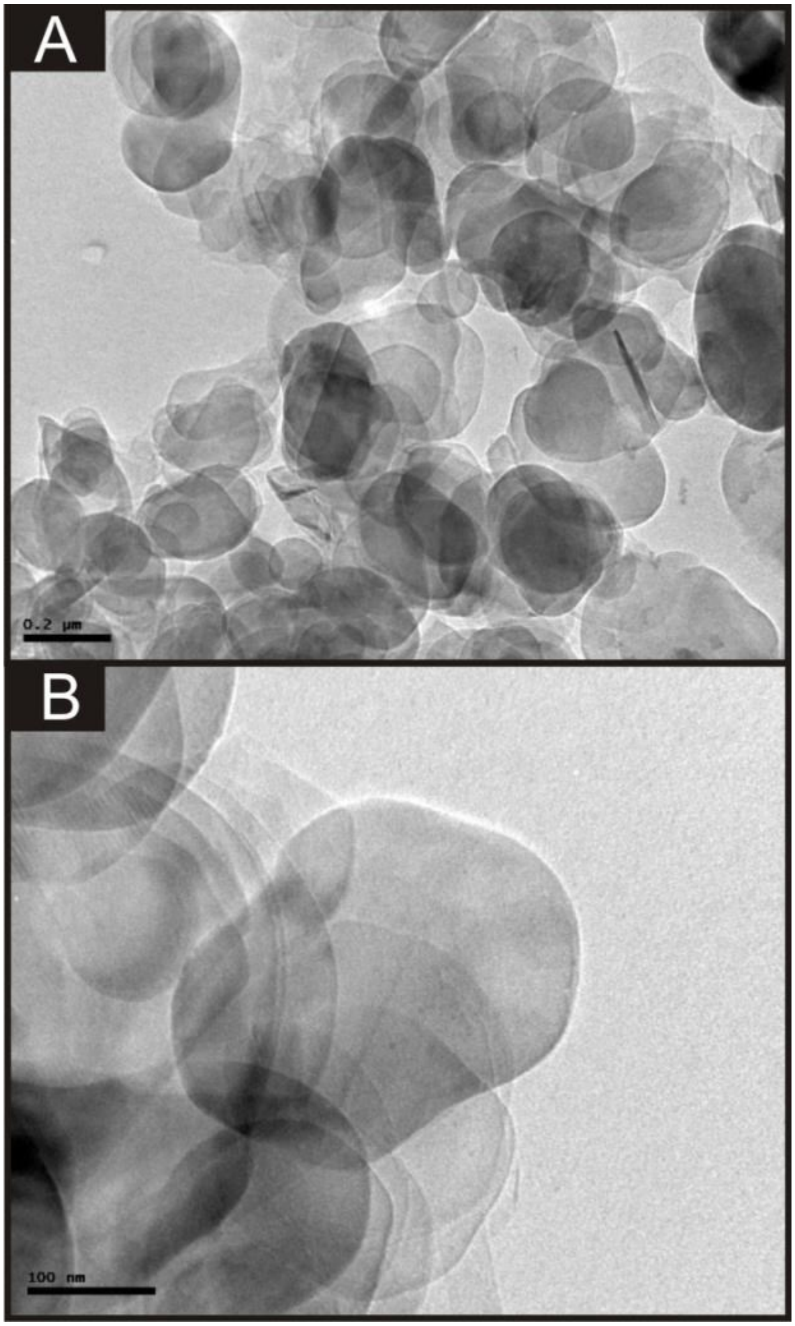

ESI Figure 11

Typical SEM image of an SPE with 324 ng pristine 2D-hBN immobilised upon the surface. Pristine 2D-hBN nanoplatelets are evident as small, disc-like shapes approximately 200 nm in size.

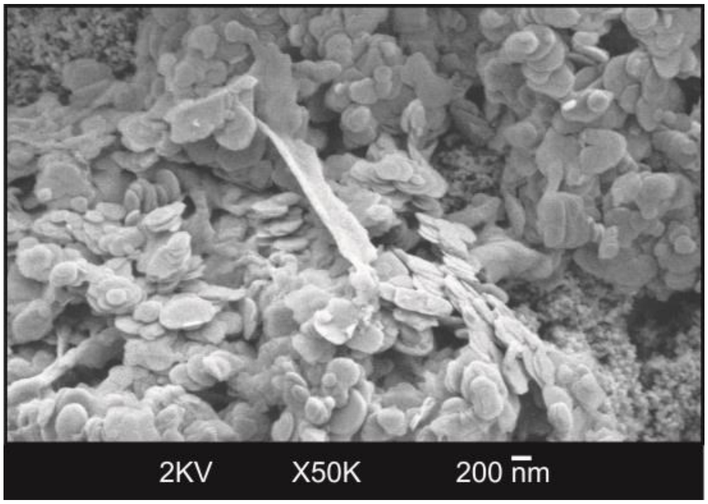

ESI Figure 12

Curve fitted XPS spectra of pristine 2D-hBN deposited upon a Si (111) wafer (dotted line). (A) illustrates XPS spectra of the B atom (solid line) and spectra (B) is that of the N atom (solid line).

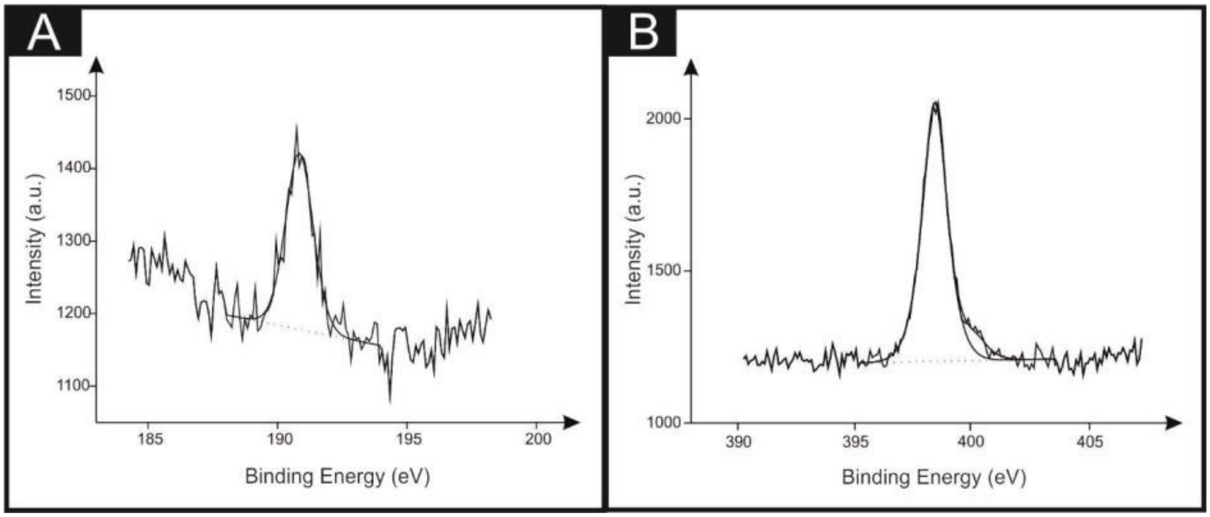

ESI Table 2

A summary depicting the composition of pristine 2D-hBN dried from ethanol suspension onto Si(111) following analysis of XPS spectra. Note that the analysis includes data from the pristine 2D-hBN, the ethanol residue, and a proportion of the surface region of the Si(111) wafer including the native surface oxide.

Element	Atom % Concentration
Na 1s	2.9
O 1s	21.2
N 1s	3.5
Ca 2p	0.5
C 1s	44.7
B 1s	3.7
Si 2p	23.5

ESI Figure 13

Typical SEM image (A) for pristine 2D-hBN immobilised upon a silicon substrate, where the red box shows the target of the EDX analysis. The SEM was obtained at ×20,000 magnification. An acceleration voltage of 25.00 kV and a working distance of 14.4 mm were utilised. Part (B) illustrates the accompanying EDX spectrum of pristine 2D-hBN and analysis of this is shown in the inset table.

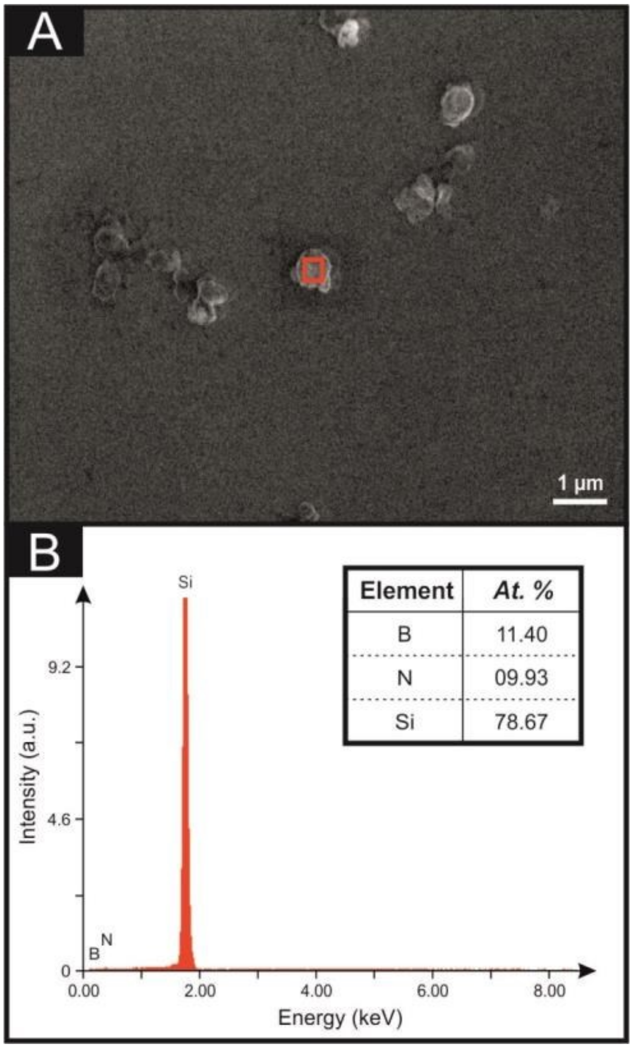

Element	*At. %*
B	11.40
N	09.93
Si	78.67

ESI Figure 14

XRD spectra of the pristine 2D-hBN deposited onto a glass slide between 5 and 45 2θ, exhibiting a characteristic peak at 26.7°.

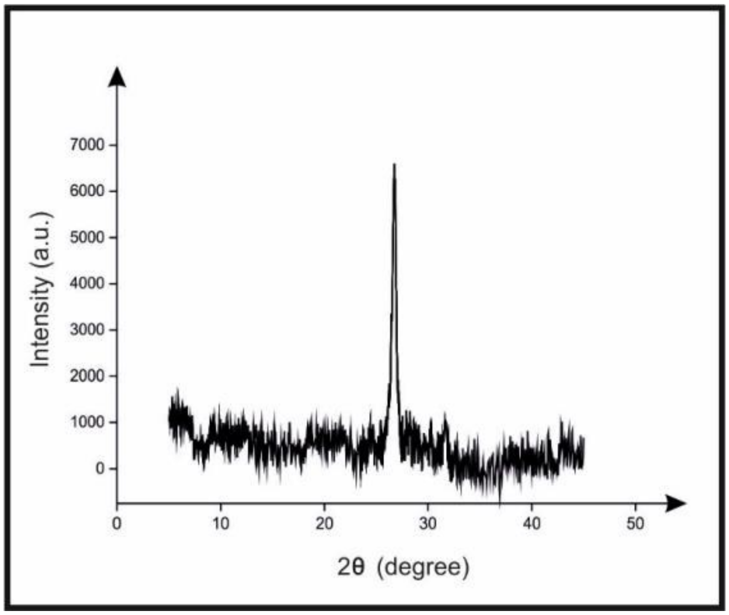

ESI Figure 15

A typical Raman spectra (A) obtained for pristine 2D-hBN (solid line) immobilised upon a supporting silicon wafer. The dotted line depicts the Raman spectra of the silicon substrate upon which pristine 2D-hBN is deposited. Image (B) shows the Raman mapping of an unmodified (bare) and a 324 ng pristine 2D-hBN modified SPE (C). Raman intensities for B and C were recorded at 1365 cm^{-1}. Figure C shows several areas, appearing as black dots, that are indicative of pristine 2D-hBN immobilisation given that the Raman intensities were recorded at the wavenumber corresponding to the peak observed in A.

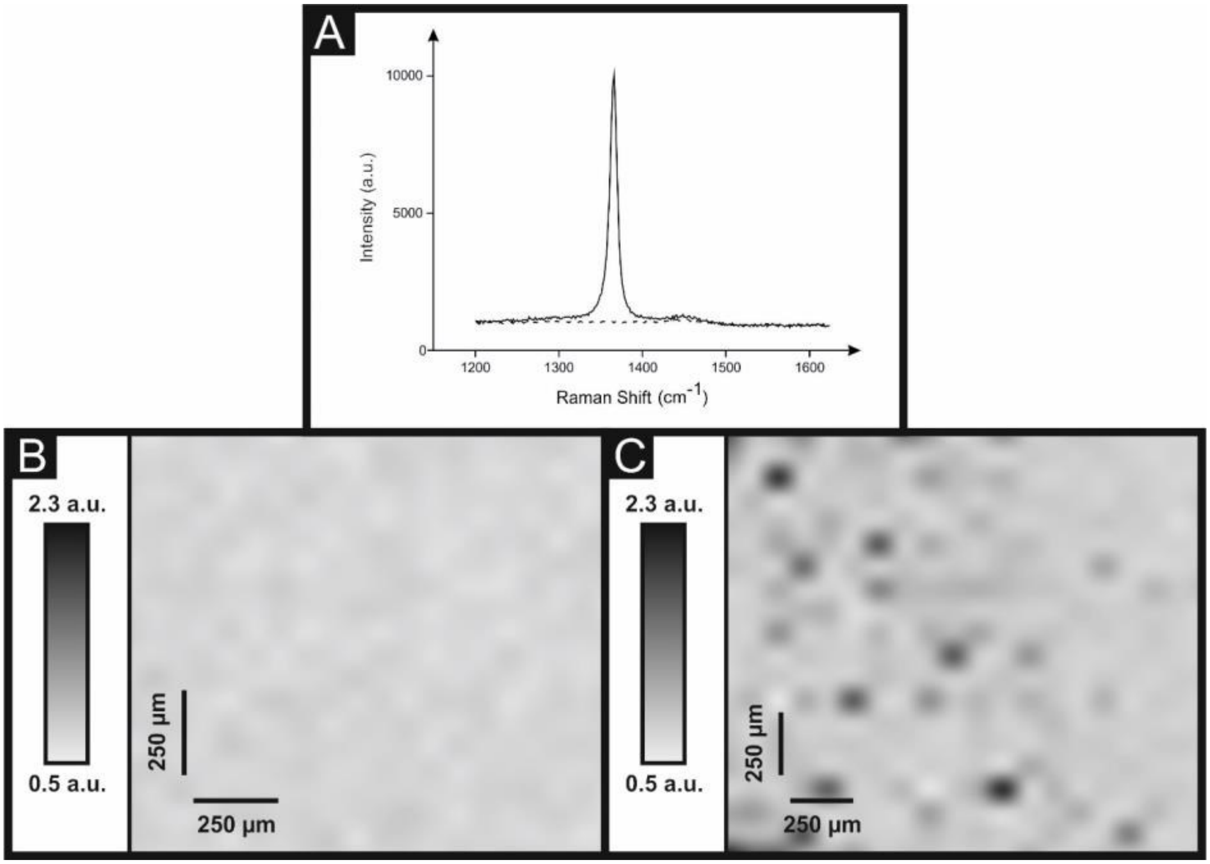

ESI Figure 16

Typical cyclic voltammograms (A) recorded in nitrogen saturated 0.1 M H_2SO_4 solution using unmodified (black line), 37.5 ng surfactant-exfoliated 2D-hBN (red line) and 10 µg sodium cholate (blue line) modified SPEs**.** Also shown are cyclic voltammograms (B) recorded in nitrogen saturated 0.1 M H_2SO_4 with unmodified (black line), 54 ng (red line), 108 ng (blue line), 216 ng (green line) and 324 ng (pink line) pristine 2D-hBN modified SPEs**.** Scan rate: 100 mV s^{-1} (*vs.* SCE).

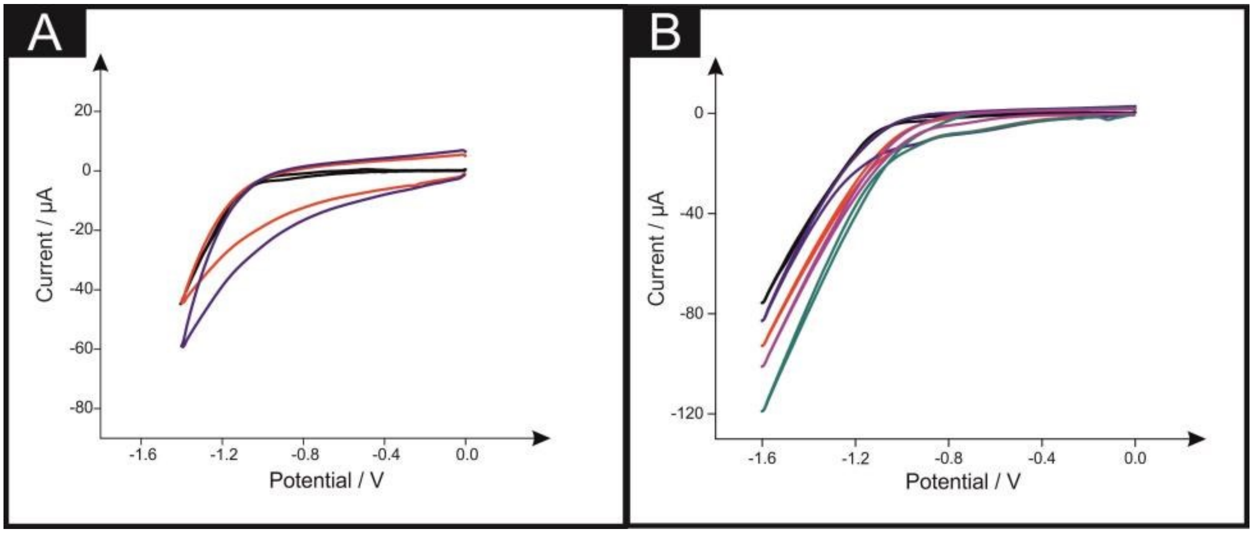

ESI Figure 17

Typical cyclic voltammograms recorded in an oxygen saturated 0.1 M H_2SO_4 solution using unmodified (black line), 54 ng (red line), 108 ng (blue line), 216 ng (green line) and 324 ng (pink line) pristine 2D-hBN modified SPEs**.** Shown in the inset is analysis of cyclic voltammograms obtained in an oxygen saturated 0.1 M H_2SO_4 solution in the form of a plot of oxygen reduction peak potential *vs.* mass of 2D-hBN electrically wired upon SPEs. Scan rate: 100 mV s^{-1} (*vs*. SCE).

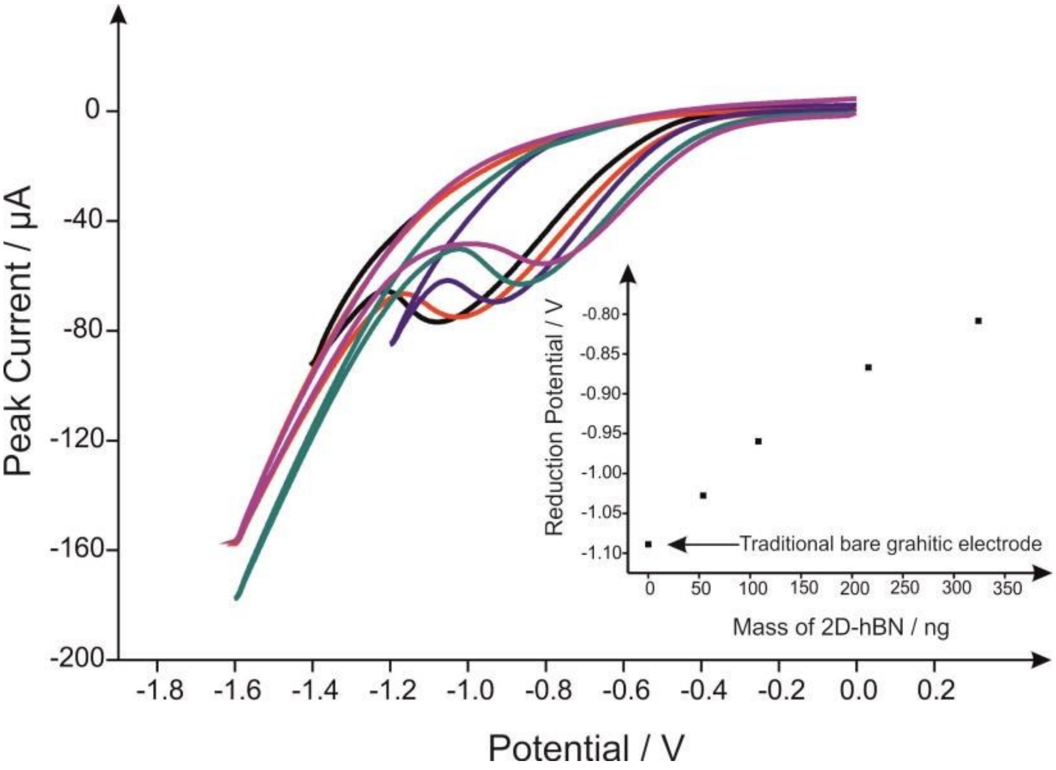

ESI Figure 18

Cyclic voltammograms recorded in 0.1 M H_2SO_4 using; (A) an unmodified SPE, (B) a 37.5 ng surfactant-exfoliated 2D-hBN modified SPE, (C) a 10 µg sodium cholate modified SPE and (D) a 324 ng pristine 2D-hBN modified SPE. Repeat scans were performed up to 10 cycles. Scan rate: 100 mV s^{-1} (*vs*. SCE).

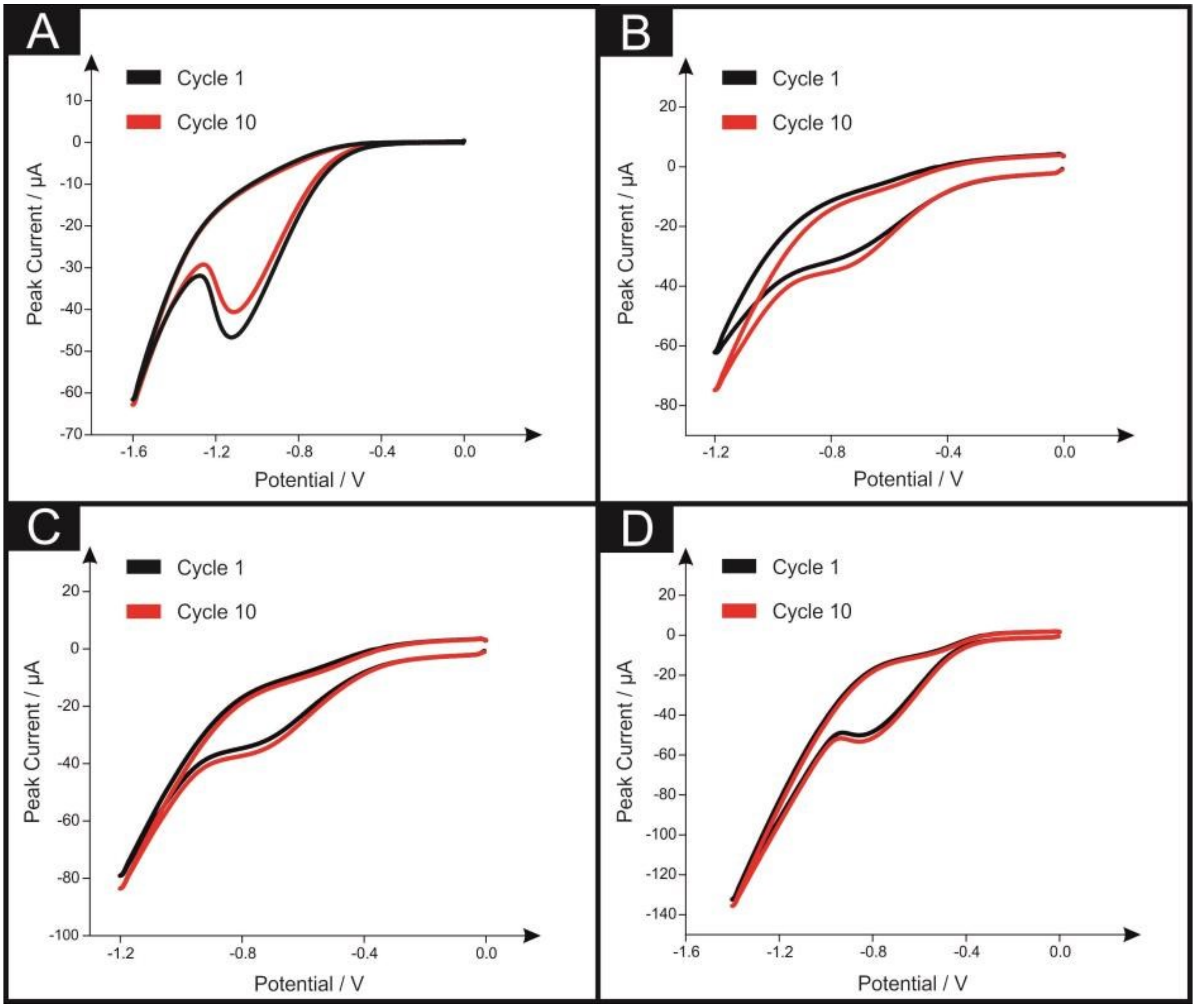

ESI Table 3

Analysis of voltammograms presented in ESI Figure 18. Table exhibits the effects of increasing voltammetric cycle number upon the ‘cathodic peak current’ (µA) and ‘cathodic peak potential’ (V) when utilising a 37.5 ng surfactant-exfoliated 2D-hBN, 324 ng pristine 2D-hBN and 10 µg sodium cholate modified SPE.

Electrode	**Cycle 1**		**Cycle 10**	
	Cathodic Peak (Reduction) Current (µA)	**Cathodic Peak (Reduction) Potential (V)**	**Cathodic Peak (Reduction) Current (µA)**	**Cathodic Peak (Reduction) Potential (V)**
37.5 ng surfactant-exfoliated 2D-hBN modified SPE	-28.80	-0.71	-32.20	-0.71
10 µg sodium cholate modified SPE	-30.70	-0.71	-32.50	-0.70
324 ng pristine 2D-hBN modified SPE	-50.40	-0.84	-53.20	-0.84
Unmodified SPE	-46.90	-1.12	-40.08	-1.11

ESI Figure 19

Typical cyclic voltammograms recorded in 0.1 M H_2SO_4 with surfactant-exfoliated 2D-hBN masses of: 7.5 (red line), 15 (yellow line), 37.5 (blue line) and 75ng (green line) immobilised upon SPEs (A). Sodium cholate masses of: 2.0 (red line), 4.0 (yellow line), 10.0 (blue line) and 20.0 µg (green line) immobilised upon SPEs (B). Pristine 2D-hBN masses of: 7.5 (red line), 15 (yellow line), 37.5 (blue line) and 75ng (green line) immobilised upon SPEs (C). In all cases, the black line represents an unmodified (bare) SPE. Scan rate: 100 mV s^{-1}.

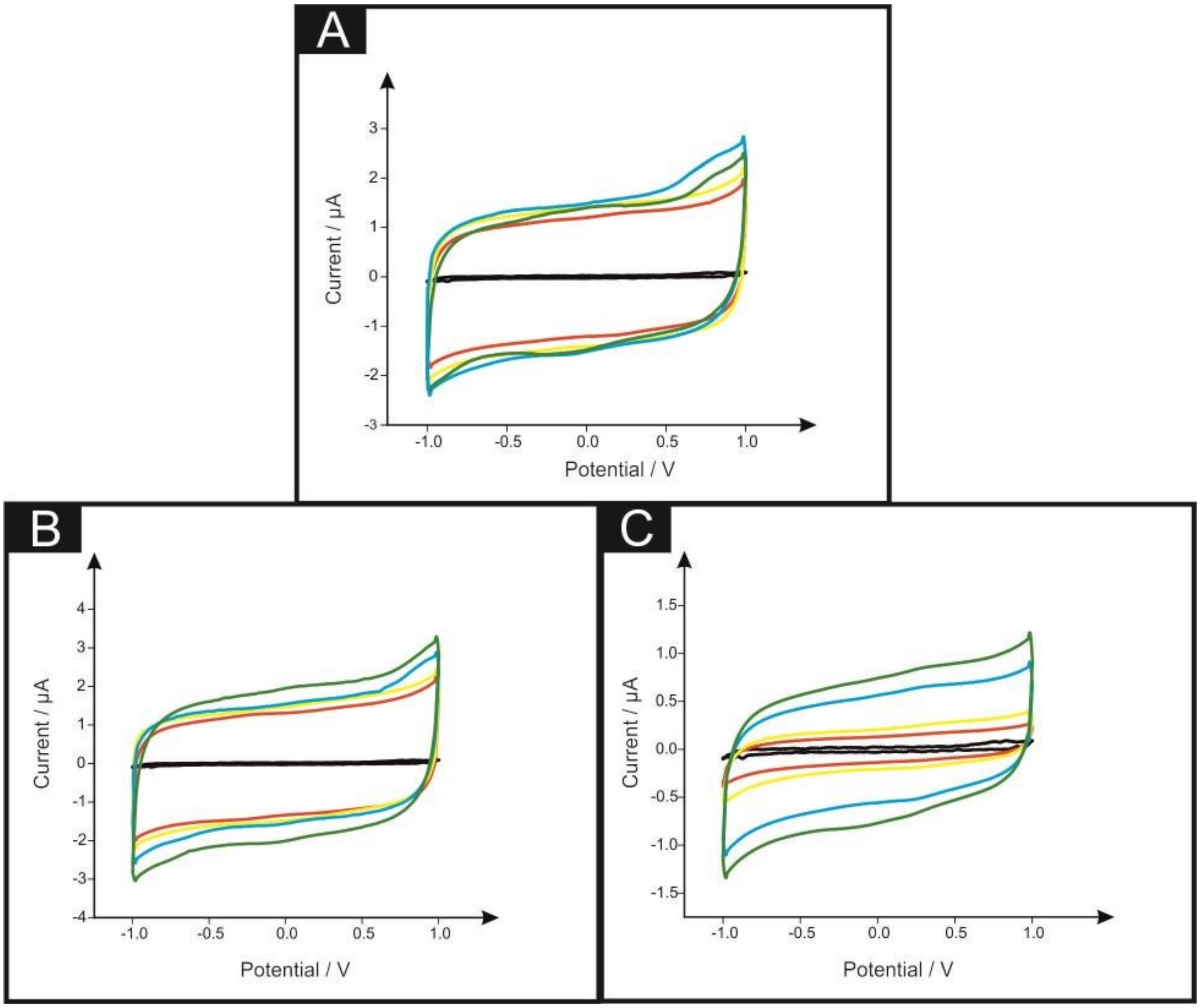

ESI Table 4

A summary of the effect of increasing mass immobilisation of pristine 2D-hBN, surfactant-exfoliated 2D-hBN and sodium cholate modified SPEs upon capacitance µF. Note, capacitance values were obtained from cyclic voltammograms.

Mass of Pristine 2D-hBN ng	Capacitance µF	Mass of Surfactant-exfoliated 2D-hBN ng	Capacitance µF	Mass of Sodium Cholate µg	Capacitance µF
0	0.24	0	0.24	0	0.24
7.50	1.55	7.5	11.90	2.0	14.08
15.0	2.46	15.0	13.80	4.0	16.00
37.5	6.33	37.5	14.90	10.0	16.70
75.0	8.28	75.0	13.55	20.0	21.07

ESI Table 5

A summary of the effect of increasing mass immobilisation of pristine 2D-hBN (7.5 - 75 ng), surfactant-exfoliated 2D-hBN (7.5 – 75 ng) and sodium cholate (2 -20 µg) modified SPEs towards capacitance (C_{WE}) µF, areal capacitance (C_A) µF cm^{-2}, volumetric capacitance (C_V) F cm^{-3} and specific capacitance (C_S) F g^{-1} . The current is held at 5.0 µA throughout. Note, capacitance values were obtained from charge/discharge profiles.

Mass of Pristine 2D-hBN ng	**Capacitance µF**	**Capacitance µF cm^{-2} (C_A)**	**Capacitance F cm^{-3} (C_V)**	**Capacitance F g-^{1} (C_S) (method 1)**	**Capacitance F g-^{1} (C_S) (method 2)**	**Capacitance F g-^{1} (C_S) (method 3)**
0	6.15	87.02	0.058	0.02	N/A	N/A
7.50	10.18	144.00	3108.63	1357.48	1357.46	537.16
15.0	10.43	147.54	1592.50	695.42	695.40	285.26
37.5	11.47	162.20	700.28	305.80	305.78	141.73
75.0	12.69	179.44	387.35	169.15	169.13	87.12
Mass of Surfactant 2D-hBN (2D-hBN ng)	**Capacitance µF**	**Capacitance µF cm^{-2} (C_A)**	**Capacitance F cm^{-3} (C_V)**	**Capacitance F g-^{1} (C_S) (method 1)**	**Capacitance F g-^{1} (C_S) (method 2)**	**Capacitance F g-^{1} (C_S) (method 3)**
0	6.15	87.02	0.058	0.02	N/A	N/A
7.5	13.09	185.09	3995.60	1744.80	1744.78	924.48
15.0	13.70	193.75	2091.27	913.22	913.20	503.06
37.5	15.39	217..65	939.67	410.34	410.32	246.27
75.0	14.15	200.24	432.26	188.76	188.74	106.73
Mass of Surfactant 2D-hBN (Sodium Cholate µg)	**Capacitance µF**	**Capacitance µF cm^{-2} (C_A)**	**Capacitance F cm^{-3} (C_V)**	**Capacitance F g-^{1} (C_S) (method 1)**	**Capacitance F g-^{1} (C_S) (method 2)**	**Capacitance F g-^{1} (C_S) (method 3)**
0	6.15	87.02	0.058	0.02	N/A	N/A
2	13.09	185.09	6.53	6.54	6.53	3.47
4	13.70	193.75	3.42	3.42	3.40	1.89
10	15.39	217..65	1.53	1.54	1.52	0.92
20	14.15	200.24	0.71	0.71	0.69	0.40
Mass of Surfactant 2D-hBN (both components g)	**Capacitance µF**	**Capacitance µF cm^{-2} (C_A)**	**Capacitance F cm^{-3} (C_V)**	**Capacitance F g-^{1} (C_S) (method 1)**	**Capacitance F g-^{1} (C_S) (method 2)**	**Capacitance F g-^{1} (C_S) (method 3)**
0	6.15	87.02	0.116	0.02	N/A	N/A
2.0075×10^{-6}	13.09	185.09	42.80	6.52	6.50	3.45
4.015×10^{-6}	13.70	193.75	22.44	3.41	3.39	1.88
1.00375×10^{-5}	15.39	217..65	10.08	1.53	1.51	0.92
2.0075×10^{-5}	14.15	200.24	4.64	0.71	0.68	0.40
Mass of Sodium Cholate µg	**Capacitance µF**	**Capacitance µF cm^{-2} (C_A)**	**Capacitance F cm^{-3} (C_V)**	**Capacitance F g-^{1} (C_S) (method 1)**	**Capacitance F g-^{1} (C_S) (method 2)**	**Capacitance F g-^{1} (C_S) (method 3)**
0	6.15	87.02	0.058	0.02	N/A	N/A
2.0	13.02	184.09	6.49	6.51	12.99	6.86
4.0	14.73	208.35	3.67	7.37	7.34	4.29
10.0	15.69	221.89	1.56	1.57	3.12	1.91
20.0	17.36	245.58	0.86	0.87	1.72	1.12

ESI Figure 20

Capacitance retention 500 life cycle test obtained from charge/discharge profiles in 0.1M H_2SO_4 utilising a 75 ng pristine 2D-hBN, 75 ng surfactant-exfoliated 2D-hBN and 10 µg sodium cholate modified SPE, at a current of 5.0 µA.

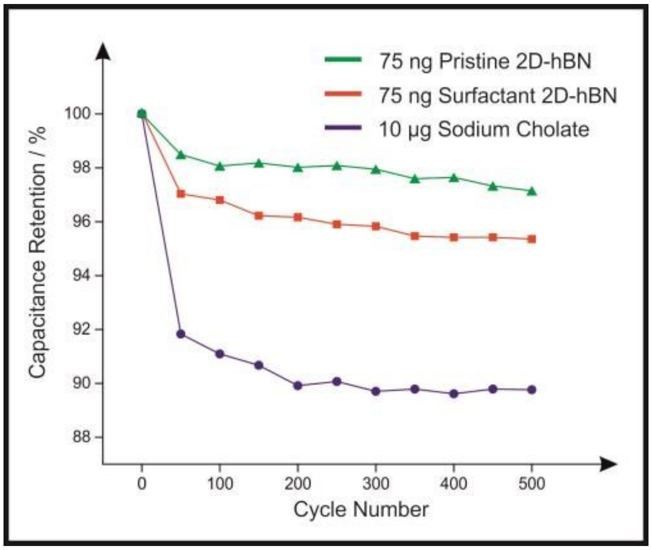

ESI Figure 21

Typical charge/discharge profiles recorded in 0.1 M H_2SO_4 with a 7.5 ng surfactant-exfoliated 2D-hBN modified SPE. Note the average slope of the charge profile relates to 0.015 V s^{-1} (*N=3*) at a current of 5.0 µA.

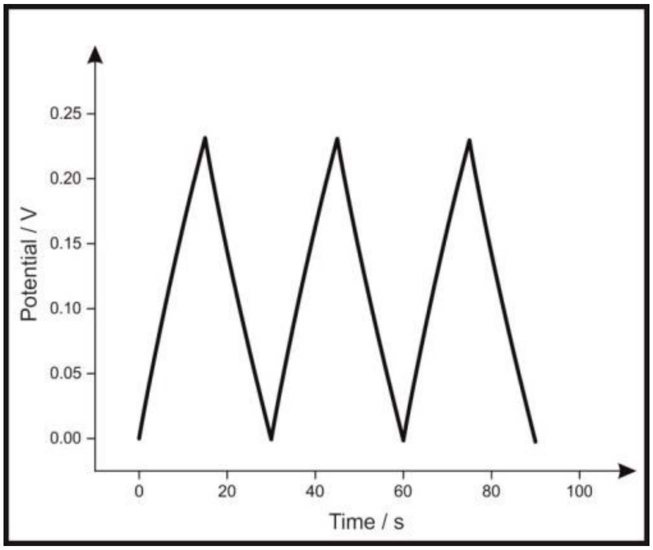

References

1. J. Tauc, R. Grigorovici and A. Vancu, *Phys. Status Solidi B.*, 1966, 15, 627-637.
2. L. Song, L. Ci, H. Lu, P. B. Sorokin, C. Jin, J. Ni, A. G. Kvashnin, D. G. Kvashnin, J. Lou, B. I. Yakobson and P. M. Ajayan, *Nano Lett.*, 2010, 10, 3209-3215.
3. Graphene Supermarket, https://graphene-supermarket.com, accessed; 04/01/2016.
4. L. Song, L. Ci, H. Lu, P. B. Sorokin, C. Jin, J. Ni, A. G. Kvashnin, D. G. Kvashnin, J. Lou, B. I. Yakobson and P. M. Ajayan, *Nano Lett.*, 2010, 10, 3209-3215.
5. C. E. Banks, A. Crossley, C. Salter, S. J. Wilkins and R. G. Compton, *Angew. Chem. Int. Ed.*, 2006, 45, 2533-2537.
6. G. R. Bhimanapati, D. Kozuch and J. A. Robinson, *Nanoscale*, 2014, 6, 11671-11675.
7. R. V. Gorbachev, I. Riaz, R. R. Nair, R. Jalil, L. Britnell, B. D. Belle, E. W. Hill, K. S. Novoselov, K. Watanabe, T. Taniguchi, A. K. Geim and P. Blake, *Small*, 2011, 7, 465-468.